ACS APPLIED MATERIALS & INTERFACES

RESEARCH ARTICLE

www.acsami.org

Electrospray Preparation of Hierarchically-structured Mesoporous TiO_2 Spheres for Use in Highly Efficient Dye-Sensitized Solar Cells

Daesub Hwang,[†,‡] Horim Lee,[†,§] Sung-Yeon Jang,[⊥] Seong Mu Jo,[†] Dongho Kim,[‡] Yongsok Seo,[§] and Dong Young Kim*[,†]

[†]Optoelectronic Materials Lab., Korea Institute of Science and Technology, Seoul 136-791, Korea

[‡]Department of Chemistry, Yonsei University, Seoul 120-749, Korea

[§]Department of Material Science and Engineering, Seoul National University, Seoul 151-744, Korea

[⊥]Department of Chemistry, Kookmin University, Seoul 136-702, Korea

Supporting Information

ABSTRACT: We report a simple method to prepare hierarchically structured TiO_2 spheres (HS-TiO_2), using an electrostatic spray technique, that are utilized for photoelectrodes of highly efficient dye-sensitized solar cells (DSSCs). This method has an advantage to remove the synthesis steps in conventional sol-gel method to form nano-sized spheres of TiO_2 nanoclusters. The fine dispersion of commercially available nanocrystalline TiO_2 particles (P25, Degussa) in EtOH without surfactants and additives is electro-sprayed directly onto a fluorine-dopoed tin-oxide (FTO) substrate for DSSC photoelectrodes. The DSSCs of HS-TiO_2 photoelectrodes show high energy conversion efficiency over 10% under illumination of light at 100 mW cm^{-2}, AM1.5 global. It is concluded from frequency-dependent measurements that the faster electron diffusion coefficient and longer lifetime of HS-TiO_2 than those in nonstructured TiO_2 contribute to the enhanced efficiency in DSSCs.

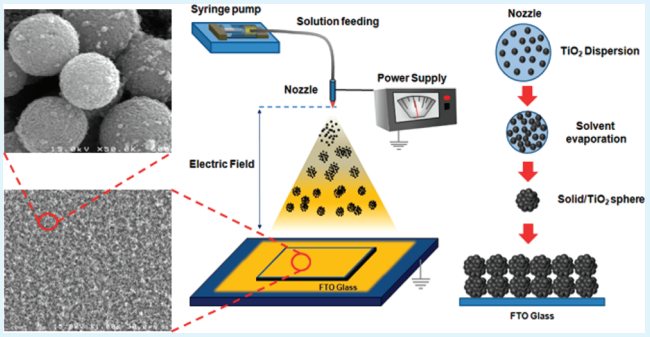

KEYWORDS: electrostatic spray, titanium dioxide, photovoltaic, solar cells, porous materials

INTRODUCTION

Dye-sensitized solar cells (DSSCs) have been under development since the Grätzel group reported the first example of highly efficient electrochemical photovoltaics. DSSCs have several advantages over other types of solar cells, such as low cost fabrication, tunability with respect to the cell color, and transparency.[1] Photoelectrodes for DSSCs transport excited electrons from the photoexcited dyes to the electron collector (FTO substrate). The critical characteristics of the photoelectrodes depend on the nature of the electrode material, particle size, morphology, electron transport and diffusion properties, surface area, and dye adsorption,[2−4] Nanocrystalline (nc-) TiO_2 particles are frequently used in DSSC photoelectrodes. The small particle size (ca. 20 nm) enables enhance the dye adsorption and exciton generation due to the relatively large surface area of the particles. However, small particles with large surface areas do not always give the best performance due to the added grain boundaries and defects on the particle surfaces, which can delay electron transport. The pore size distribution at the electrode surface influences the permeation and diffusion of electrolytes at the surface. Pore size also influences the uniformity of the surface after calcination steps because of crack propagation, which increases the possibility of recombination reactions with electrolytes, resulting in shortened electron lifetimes.[5,6]

The surface area of the granular particles that form the electrodes, which is correlated with the number of grain boundaries, electron transport properties, and extent of dye adsorption, has been optimized previously to yield particles of diameter 15−20 nm.[7−9] The various TiO_2 shapes were also investigated using metal oxide one-dimensional (1D) structures in the form of nanofibers,[10] nanowires,[11,12] nanotubes,[13,14] and nanorods.[15] The 1D structured materials provided more efficient pathways for electron injection from the excited dyes to the conduction band of the TiO_2 particles because of fewer grain boundaries than were present in non-1D particles[14,16−18] However, dye adsorption onto the 1D TiO_2 particles was decreased compared to the nc-TiO_2s due to the reduced surface area. The resulting photocurrent generation was generally low.[12] In previous studies by our group, however, nanorod electrodes were developed that possessed relatively large surface areas and yielded high photocurrents.[14,15] Recently, several groups have reported zero-dimensional (0D) hierarchical structures as optimal morphologies for DSSCs.[17,19,20] The 0D hierarchically-structured TiO_2 (HS-TiO_2) were suggested as the most promising photoelectrodes

Received: April 28, 2011
Accepted: June 6, 2011
Published: June 06, 2011

for DSSCs due to the advantages of (1) large surface area and dye adsorption; (2) fast electron transport at reduced grain boundaries; (3) light scattering effects of the submicrometer sized structures; and (4) better penetration of electrolytes through the relatively large pores between spheres.[17,19−22] We note that it is not simple to obtain such hierarchical structures using multi-step processes, such as the sol−gel method,[20] solvothermal reactions,[21] hydrolysis,[17] or the electrospinning of nanorods.[15] These processes are not practical or cost-effective for the large-scale production of DSSC modules.

The electrostatic spray (e-spray) technique has recently been considered as a cheap and simple process to directly deposit thin films from their colloidal solutions. The techniques can be applied widely in modern material technologies, microelectronics, nanotechnology,[23] and industries for the deposition of various ceramic powders, polymer powders,[24] and TiO_2 electrodes for DSSCs.[5,25−27] During e-spray deposition known as induction or conduction charging, the droplets can be charged of their atomization by mechanical forces in the presence of electric field between the solution and the depositing substrates.[28] The electric field develops an electric charge on the liquid surface and the charge is carried out by the droplets detaching from the jet. The advantage of the e-spray is that droplets are highly charged, up to a fraction of the Rayleigh limit. The Rayleigh limit is the magnitude of charge on a drop, which overcomes the surface tension force that leads to the drop fission. The magnitude of the charge on a droplet is given by the equation, $Q_R = 2\pi(16\sigma_l\varepsilon_0 r^3)^{1/2}$, where σ_l is the liquid surface tension, ε_0 is the dielectric permittivity of the free space, and r is the droplet radius.[23] The deposition efficiency of the charged droplets is usually much higher than that of the uncharged droplets, which can improve the adhesion between the materials and substrates. The e-spray process is generally performed at room temperature under atmospheric pressure, which leads to a low equipment cost. Although e-spraying is well-reputed as a highly efficient coating and painting process, little attention has been devoted to applying it in the field of thin-film electronic devices.[29]

EXPERIMENTAL SECTION

Preparation of Hierarchically Structured TiO_2 Nanosphere (HS-TiO_2). the 10 wt % P-25(Degussa) nc-TiO_2 was dispersed in ethanol by using an ultra apex mill (Model UAM-015, Kotobuki). The dispersed solution was loaded into a plastic syringe which was connected to a high voltage power supply (BERTAN SERIES 205B). Then, the dispersed P25 solution was electrosprayed directly onto the conducting FTO substrates (10 cm × 10 cm).

To prepare the hierarchically-structured TiO_2 sphere with a diameter of about 640 nm, the electric field of 15 kV was applied between the metal orifice and the conducting substrate. The feed rate was controlled by a syringe pump at 35-30 μl/min. In order to form a uniform thickness in a large area, the nozzle and the substrate were placed on the motion control system with a microprocessor. On the other hand, non-structured TiO_2 layers were prepared at the 5 kV electric field with 10 wt % P25 powder dispersed in ethanol/water (7/3 v/v) solution. Surface area were determined by the Brunauer−Emmett−Teller (BET) method and pore volume and size distributions were determined by the Barrett−Joyner−Helenda (BJH) method using the adsorption branches of the isotherms.

Device Fabrication. After electrospraying process, the as-prepared TiO_2 electrode was put between two planar steel plates. Typical pressures used for efficient solar cell were 12 MPa for FTO substrates at 120°C for 10 min. The photoanodic electrodes coated with hierarchically-structured TiO_2 spheres were sintered under air condition at 500°C for 30 min. For the post-treatment with 0.05M $TiCl_4$ aq. solution, the TiO_2 films were soaked for 20 min at 80°C and were rinsed with water and then sintered again at 450 °C for 30 min. After cooling to 80 °C, the TiO_2 electrodes were immersed into the purified 3×10^{-4} M *cis*-di (thiocyanato)-*N*,*N*′-bis (2,2′-bipyridyl-4-carboxylic acid-4′-tetrabutylammonium carboxylate) ruthenium(II) (N719, Solaronix) solution for 15h at room temperature.

For the counter electrode, the FTO plates were drilled by microdrill, washed with 0.1M HCl solution in ethanol, and then subsequently cleaned in an ultrasonic bath with water and ethanol for 15 min. A Pt counter electrode was prepared by drop casting of 5 mM H_2PtCl_6 in isopropyl alcohol onto the washed FTO plates and then sintered at 400°C for 20 min under air condition. The dye-adsorbed TiO_2 electrodes were rinsed with ethanol and dried under nitrogen flow. The dye-adsorbed TiO_2 electrodes were assembled and sealed with the counter electrode using the thermal adhesive films (Surlyn, Dupont 1702, 25-μm-thick) as a spacer to produce sandwich-type cells. The liquid electrolyte consisted of 0.7 M 1-propyl-3-methylimmidazolium iodide (PMII), 0.03 M iodine (I_2), 0.1 M guanidiniumthiocyanate (GSCN), and 0.5 M 4-*tert*-butylpyridine (TBP) in a mixture of acetonitrile (ACN) and valeronitrile (VN) (85/15 v/v). An electrolyte solution was introduced through a drilled hole on the counter electrode. Finally, the holes were sealed with a hot-melt films and a cover glass.

Photovoltaic and Photoelectrical Measurements. Photovoltaic measurement of the DSSCs employed an AM 1.5 solar simulator between the sample and a 450 W Xe lamp. The intensity of the simulated light was calibrated by a Si reference solar cell equipped with a BK7 filter for approximating AM 1.5 global radiation. The photovoltaic characteristics of DSC were obtained by applying an external potential bias to the cells and measuring the generated photocurrent with a keithley model 2400 source meter. The photovoltaic performance was measured by using black tapes with an aperture area of 0.35 cm^2. IPCE was measured as a function of wavelength from 350 nm to 800 nm using a specially designed IPCE system for dye-sensitized solar cell (PV measurement, Inc.). A 75 W xenonlamp was used as the light source for generating a monochromaticbeam. Calibration was performed using a NIST-calibrated silicon photodiode as a standard. IPCE values were collected at a low chopping speed of 5 Hz. The electrical impedance spectra were measured using an impedance analyzer (Solatron 1260) at an open-circuit potential under AM 1.5 full sun illumination(100 mW/cm^2), with a frequency range of $0.1-10^5$ Hz. The magnitude of the alternative signal was 10 mV. Impedance parameters were determined by fitting of the impedance spectra using Z-plot software. The electron transport time and electron recombination lifetimes were measured by intensity-modulated photocurrent spectroscopy (IMPS) and intensity-modulated photovoltage spectroscopy (IMVS). A diode laser with variable power and modulation control (Coherent Lab-laser, 10 mW, 635 nm) was used as the light source for these studies. Illumination was always incident on the working electrode side of the solar cells. The intensity was measured using a calibrated Si-photodiode. IMVS was performed under open-circuit conditions. The output of the solar cell was connected directly to a frequency response analyzers(FRA) Solatron 1260 Impedance/Gain - Phase Analyzer). IMPS was performed by connecting the solar cell via a potentiostat amplifier (EG&G PAR 273) to the FRA. During the IMVS and IMPS measurements, the cell was illuminated with sinusoidally modulated light having a small ac component (10% or less of the dc component)

RESULTS AND DISCUSSION

In the present study, a novel and simple method was developed for the preparation of mesoporous HS-TiO_2 using the e-spray process from a dispersion of commercially available

Scheme 1. Schematic Diagram of (a) Electrostatic Spray and (b) Formation of Hierarchically Structured TiO_2 Nanospheres

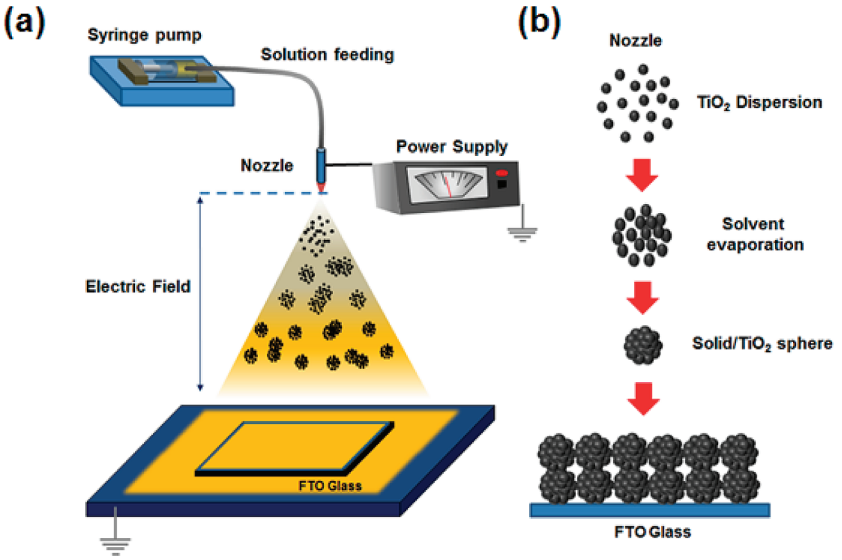

nc-TiO_2 primary particles (P-25, Degussa). In addition, the dispersed TiO_2 solutions synthesized by hydrothermal methods can be used for the e-spray process to prepare the HS-TiO_2 based photoelectrodes. The photoelectrode for DSSCs could be obtained directly in one step on an FTO substrate. The nc-TiO_2 dispersion did not contain additives, such as surfactants or stabilizers, with the exception of ethanol as a dispersion medium. Therefore the process can be simply applied to fabrication of flexible or low temperature DSSCs. Furthermore, e-spray was also used for production of diverse sized nanoclusters. The charge and size of the droplets can be controlled to some extent by manipulating the flow rate, the applied voltage applied to the nozzle, and changing the concentration of suspended substances. Thus, we established that the diameters of the HS-TiO_2 could be controlled from 200 nm to the micrometer scale by changing the process parameters. The fabrication of efficient DSSC devices has never been reported using the e-spray method despite its rapid preparation of the HS-TiO_2. The power conversion efficiencies of the e-sprayed electrodes exceeded 9.5% with illumination through a photo-mask at an illumination power of AM1.5 global at 100 mW cm^{-2} (see Figure S1 in the Supporting Information).

Scheme 1 shows the schematic diagram of e-spray for DSSCs. Namely, the e-spray method for the preparation of photoelectrodes possesses the several advantages over conventional coating methods, such as the doctor blade or screen-printing methods. Firstly, the TiO_2 photoelectrodes were formed by e-spray from a binder-free TiO_2 dispersion that contained only TiO_2 nanoparticles and ethanol. For the preparation of plastic DSSCs, the sintering process at 500°C could be eliminated from the process. At second, the e-spray techniques have been adopted in industries because the low cost, simple coating processes are applicable over large areas, can be easily scaled-up, and proceed at a high deposition rate.

To prepare the HS-TiO_2s as shown in Figure 2d, the solution and processing conditions were sufficiently optimized for the e-spray method. The saturation vapor pressure of the solvent was required to be low (as was the case for ethanol) so that spheres would form. The TiO_2 primary particles had to be well dispersed

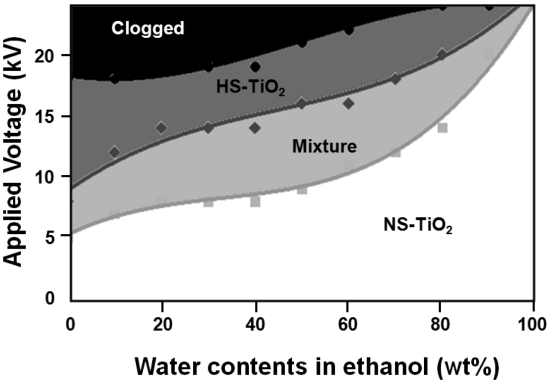

Figure 1. Phase diagram of the electrospray parameters, the applied voltage vs. the water contents in EtOH at a distance of 10 cm between the nozzle and FTO substrate.

with diameters not exceeding 70 nm of TiO_2 nanoaggregates. We adopted a micro-bead mill (with 50μm zirconia beads) to obtain dispersions that were stable for several months. The electric field between the nozzle tip and the grounded substrate exceeded 1.5 $kVcm^{-1}$. At lower electrical fields, the solvent did not evaporate fully before the particles reached to the substrate, resulting in the deposition of non-spherical TiO_2 (NS-TiO_2) particles.

Figure 1 shows the phase diagram according to the electrospray parameters, the applied voltage vs. the water contents in EtOH at a distance of 10 cm between the nozzle and FTO substrate. The phase statues are divided into the four sections according to the applied electric field. At a certain water content, the phases change with increasing the electric fields as (1) the non-sphere formation, (2) mixed zone (non-spheres and spheres, see the Supporting Information Figure S2) (3) HS-TiO_2 spheres, and (4) unable to spray due to clogging the nozzle. In order to obtain HS-TiO_2 spheres, the electrical field was applied carefully referring to the phase diagram. For examples, the HS-TiO_2 layers as shown in images d and e in Figure 2 were prepared from the EtOH only dispersion at 15 kV applied voltage

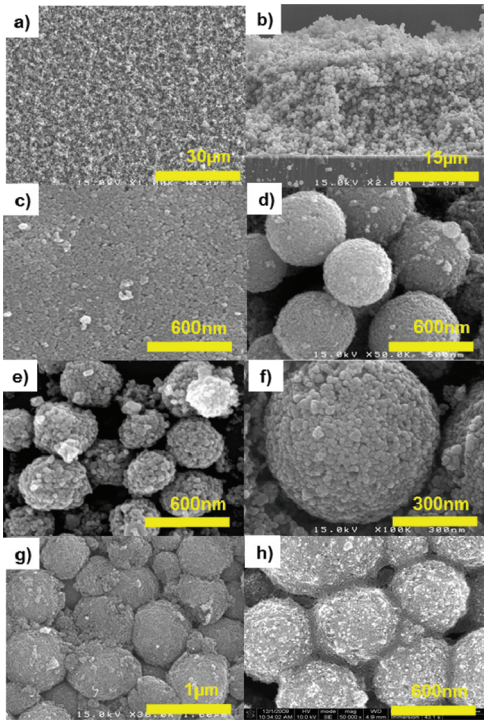

Figure 2. SEM image of (a) crack-free photoelectrode composed of hierarchically-structured (HS-) TiO_2 spheres at 1000x magnification, (b) cross-sectional image of the HS-TiO_2 layer, (c) the non-structured (NS-) TiO_2 layer by electrospray, (d) the HS-TiO_2 (dia. 640 nm), (e) dia. 260 nm, (f) an enlarged image of a HS-TiO_2 as nanoclusters of P25, (g) after hot-pressing at 120°C (12 ton for 10 min), and (h) post-treated HS-TiO_2 layer with $TiCl_4$ aq. solution.

and a non-structured surface (Figure 2c) was formed from a mixture of ethanol/water (7/3) (v/v) with an applied voltage of 5 kV. Furthermore, the sphere size was controlled by changing the TiO_2 concentration in the dispersion solution (Figure 2d,e). The quality of the TiO_2 photoelectrode layer remained intact during the conventional thermal sintering process because the e-spray process proceeded using a TiO_2 nanoparticle dispersion that did not contain binder polymers frequently used in conventional paste methods (for example, doctor blading or screen-printing). Thus, the surface of the e-sprayed TiO_2 layer was uniform and without cracks, unlike the surfaces produced using paste methods as shown in Figure 2a (also see the Supporting Information, Figure S3).

Figure 2b shows the cross-sectional image of an e-sprayed electrode (~17 μm thick) that demonstrates the uniform shape of the spheres from bottom to top. Furthermore, the e-sprayed spheres in this study formed a filled sphere instead of a hollow-shape. This was due to the fact that the spheres were formed by the ultrafast evaporation of solvent, which had a relatively high vapor pressure at the surface of the uniformly sized fine droplets containing TiO_2 nanoparticles. Thus, this generated the high convection forces that facilitated tight clusters.

A comparison of the hierarchically structured TiO_2 spheres (HS-TiO_2) (Figure 2d) with the NS-TiO_2 particle layer (Figure 2c) clearly confirmed the differences in pore volume. Figure 3 shows the Barrett–Joyner–Halenda (BJH) measurement results, both for HS- and NS-TiO_2 electrodes. The NS-TiO_2 was composed mostly of micropores. In contrast, the HS-TiO_2 spheres clearly showed additional smaller micropores

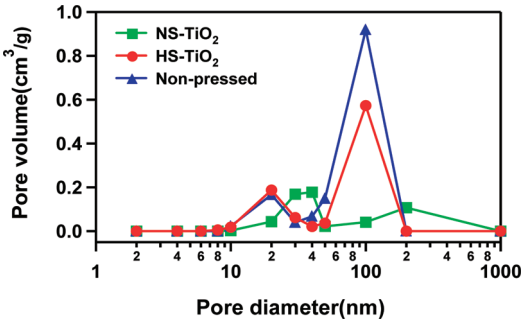

Figure 3. Pore volume distribution of HS-TiO_2 (dia. 640 nm) and NS-TiO_2 spheres. The specific surface area was estimated using the Brunauer–Emmett–Teller (BET) analysis and the pore diameters were determined by the BJH analysis using the N_2 adsorption-desorption of the isotherms.

Table 1. Physical Characteristics of the NS-TiO_2 and HS-TiO_2 (dia. 640 nm) Prepared by Electrospray

TiO_2 type	surface area ($m^2\ g^{-1}$)	pore volume ($cm^3\ g^{-1}$)	absorbed dye (mol mg^{-1})
NS-TiO_2	56.0	0.61	3.98×10^{-8}
HS-TiO_2 (as-sprayed)	76.7	1.37	4.13×10^{-8}
HS-TiO_2 (pressed)	63.7	0.91	4.06×10^{-8}

and more mesopores. The micropores in the HS-TiO_2 layer were smaller than in the NS-TiO_2 layer, suggesting that primary particles inside the HS-TiO_2 were more interconnected than those in NS-TiO_2. Also, the existence of such mesopores improved the electrolyte penetration.[20] The e-sprayed photoelectrodes were operated in mechanical-pressing process to enhance the external connection among the HS-TiO_2s, as shown in Figure 2e. The pore volume was reduced from 1.37 to 0.91 $cm^3\ g^{-1}$ after the pressing treatment. Nevertheless, these pore volumes were still larger than those of NS-TiO_2. The HS-TiO_2 based photoelectrodes with larger pore volumes provided better penetration of electrolytes and better electron diffusion. As shown in Table 1, the surface areas were 76.7 and 63.7 $m^2\ g^{-1}$ for as-sprayed and pressed TiO_2, respectively. The surface area of NS-TiO_2 was 56.0 $m^2\ g^{-1}$. The amounts of dye adsorbed onto each of the various TiO_2 layers were 3.98×10^{-6}, 4.13×10^{-6}, and 4.06×10^{-6} mol mg^{-1} for NS-TiO_2, as-sprayed HS-TiO_2, and pressed HS-TiO_2s, respectively. The dye molecules penetrated the cores of the spheres, as determined by energy dispersive x-ray spectroscopy (EDS). The SEM and EDS scans for Ru atoms in the dye-adsorbed TiO_2 spheres were performed after etching away half of the spheres using a focused ion beam (FIB). The Ru concentration was constant through the spheres, from the shell to the core regions (see the Supporting Information, Figure S4).

The photovoltaic properties of the DSSCs formed using each of the various TiO_2 photoelectrodes are summarized in Figure 4a and Table 2. HS-S and HS-L denote the hierarchically structured HS-TiO_2 spheres with average diameters of 260 and 640 nm, respectively. DSSCs from HS-TiO_2 showed better performance than DSSC from NS-TiO_2 with an active area of 0.25 cm^2 as shown in Table 2. In particular, the short circuit current density (J_{SC}), which is 15.72 mA cm^{-2} of HS-L, increased by 25% relative to that of NS-TiO_2 as 12.59 $mAcm^{-2}$. The hierarchically structured TiO_2 spheres showed remarkable improvements in

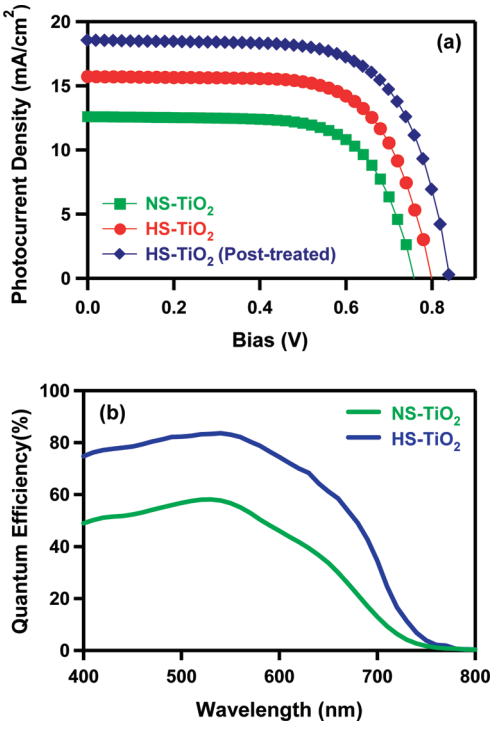

Figure 4. Photovoltaic properties of (a) the $J-V$ curves measured under simulated AM 1.5G one sun light intensity (b) incident photon to current conversion efficiency (IPCE) spectra of the DSSCs based NS-, HS-TiO_2 (dia. 640 nm) photoelectrodes.

Table 2. Summary of Photovoltaic Properties of the DSSCs Using Diverse TiO_2 Photoelectrodes Made from P25 Nanoparticles (Degussa)

sample	V_{OC} (V)	J_{SC} (mA/cm^2)	*FF*	eff (%)
HS-L (640 nm)	0.798	15.72	0.680	8.54
HS-S (260 nm)	0.782	14.39	0.677	7.61
NS-TiO_2	0.757	12.59	0.680	6.49
HS-TiO_2 (treated)	0.840	18.53	0.679	10.57
treated (with Mask)	0.834	16.68	0.689	9.59

the photocurrent generation. Similar results were reported by Kim et al.[20] and Chen et al.[19] for the TiO_2 spheres with mesopores obtained by a different synthetic route through several steps.[19,20]

The significant improvement of photocurrent in the HS-TiO_2 photoelectrodes was investigated through electrochemical impedance analysis (EIS) and intensity-modulated photocurrent spectroscopy (IMPS).[30,31] The EIS data were compared for two samples: HS- and NS-TiO_2 photoelectrodes in panels b and c in Figure 5. Each EIS showed two semicircles with a contact series resistance in the FTO substrate (R_s) of 3.65Ω for both samples. The first semicircle, designed for the high frequency range in Figure 5b, yielded the impedance at the counter electrode (R_c) for the reduction reaction of I_3^- ions in electrolytes using Pt catalysts on the counter electrode. The second semicircle, designed for the middle frequency range, showed charge transfer impedance (R_{ct}) at the interface among the electrolytes, dyes, and TiO_2. Similar R_c values were obtained, 4.2 Ω and 4.15 Ω for HS- and NS-TiO_2s, respectively.[30,32] However, the R_{ct} values showed large differences: 9.19Ω and 16.2Ω between HS- and

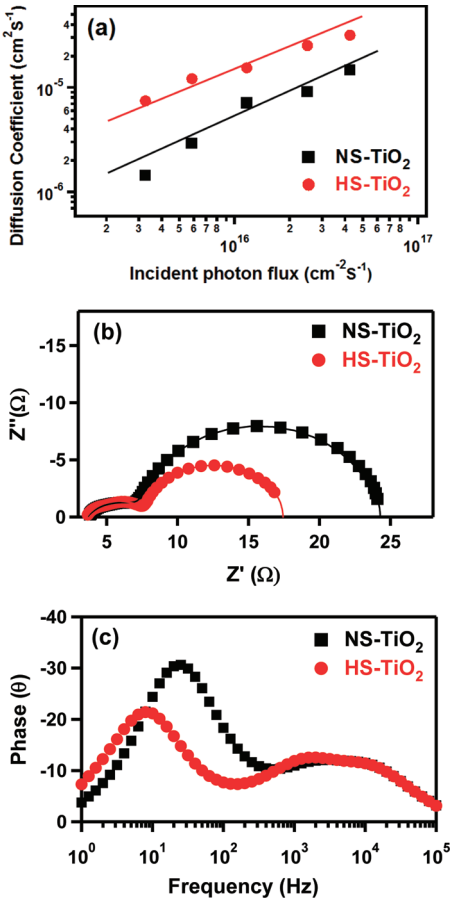

Figure 5. Electrochemical properties of (a) electron diffusion coefficient as a function of incident photon flux by intensity-modulated photocurrent spectroscopy (IMPS), (b) the nyquist plot, and (c) the bode plot measured by EIS analyzer of the DSSCs based NS-, HS-TiO_2 (dia. 640 nm) photoelectrodes. (– fitted line).

NS-TiO_2 photoelectrodes, respectively. As expected, BJH analysis showed that the interconnections among HS-TiO_2 spheres were better than among NS-TiO_2 sphere photoelectrodes. Also, the large portion of mesopores in HS-TiO_2 contributed to better diffusion of the electrolytes, which produced a improvement of charge collection efficiency (η_{cc}). The η_{cc} of DSSCs is determined by the relation; where $\eta_{cc} = 1 - \tau_d/\tau_r$, τ_d is a charge transport time and τ_r is a charge recombination lifetime.[18,33] Fast electron transport in HS-TiO_2, as confirmed using IMPS, as shown in figure 5a. The diffusion coefficient was calculated from the IMPS according to the equation $D = d^2/(2.5\tau_d)$, where D, d, and τ_d were defined as the diffusion coefficient, thickness of the TiO_2 layer, and electron transport time ($\tau_d = 1/2\pi f_{min,IMPS}$) from IMPS, respectively.[34−36] The diffusion coefficients in HS-TiO_2 were 2−3 times in the measured photon flux range faster than those in NS-TiO_2 for the TiO_2 layer thickness of $d = 10\mu$m over the range of input photon intensities, as shown in Figure 5a. The bode phase plots (frequency vs. phase angle) of the EIS results for two photoelectrodes comprising HS-and NS-TiO_2 shown in Figure 5c. The impedance at the interface between the electrolytes, dye, and TiO_2 appeared in the middle frequency range. The characteristic frequencies at the peaks were 7.9 Hz and 25.1 Hz for HS- and NS-TiO_2, respectively. From the characteristic frequency, f_{max} was related to the electron lifetime,

τ_r, as $\tau_r = 1/2\pi f_{max}$.[31,37] The lifetime of the HS-TiO_2 photoelectrode was three times longer than that of the NS-TiO_2 photoelectrode. Therefore, the 44% decrease in R_{ct}, larger charge collection efficiency, and diffusion cefficients in the HS-TiO_2 photoelectrode contributed to the 25% increase in photocurrent generation.[20,38,39]

The maximum frequency (ω_{max}) at the middle range of bode phase plots (as shown in Figure 5c) for the HS-TiO_2 based DSSCs is much lower than those for NS-TiO_2 based DSSCs, which is reliable with the tendency of the inverse open-circuit voltage (V_{OC}). Under the illumination state, the V_{OC} related to the recombination lifetime can be described in eq 1,

$$V_{oc} = \frac{RT}{\beta F} \ln\left(\frac{AI}{n_0 k_1 [I_3^-] + n_0 k_2 [D^+]}\right) \quad (1)$$

where R is the molar gas constant, T is the temperature, F is the faraday constant, β is the reaction order for I_3^- and electrons, A is the electrode area, I is the incident photon flux, n_0 is the concentration of electronic states in the conduction band, k_1 is the reaction constant for the back-reaction of the injected electron with triiodide, and k_2 is the reaction constant for recombination of electrons with oxidized dye (D^+).[30] Assuming that the recombination with the oxidized dye molecules can be neglected, the V_{OC} will depend logarithmically on the kinetic constant of the backreaction of the injected electrons with triiodide (k_1) due to the concentration of triiodide in electrolyte and incident photon flux were constant under our experimental conditions. Therefore, the V_{OC} is proportional to $\ln(1/\omega_{max})$, which demonstrates that the DSSCs with a longer lifetime was expected to have a higher V_{OC} according to eq 1. Therefore, A three-fold extended lifetime for the HS-TiO_2 photoelectrode would produce an increase in V_{OC} to yield 798 mV, compared to a V_{OC} for NS-TiO_2 of 757 mV. The increase in lifetime was related to the decreases possibility of multiple trapping as well as to the reduced recombination reactions with electrolytes. Finally, after treating the hierarchically-structured TiO_2 spheres with $TiCl_4$ and HCl aq. solution,[40,41] the V_{OC} increased to 840 mV and the power conversion efficiency reached 10.57%, in conjunction with the N719 dye, under 100 mW cm^{-2} AM1.5 global illumination (9.59% with the mask, except for the active area).

CONCLUSIONS

In this study, the e-spray method for the preparation of photoelectrodes possesses the several advantages over conventional coating methods, such as the doctor blade or screen-printing methods. At first, the e-spray method yields good adhesion between the TiO_2 layer and the substrate due to stacking of the highly charged particles under the strong applied electric field. Secondary, the TiO_2 photoelectrodes were formed from a binder-free TiO_2 dispersion that contained only TiO_2 nanoparticles and ethanol. Therefore, for the preparation of plastic DSSCs, the sintering process at 500 °C could be eliminated from the process. Thirdly, the e-spray techniques have been adopted in industries because the simple coating processes are applicable over large areas, can be easily scaled-up, and proceed at a high deposition rate. Fourthly, this method provided a simple and cost-effective process by eliminating hydrothermal reactions. The hierarchically-structured spheres formed mesopores during the electrospray process, which improved the efficiency of the DSSC because of the advantages conveyed by sphere-shaped particulate electrodes, for example, the large surface area, scattering effects, and large porosity, among other advantages, which contributed an increase in power conversion efficiency of the DSSCs. The e-spray method in this study is a candidate for simple method for forming hierarchically structured spheres with mesopores.

ASSOCIATED CONTENT

Supporting Information. This material is available free of charge via the Internet at http://pubs.acs.org.

AUTHOR INFORMATION

Corresponding Author
*E-mail: dykim@kist.re.kr. Tel: +82- 2- 958-5323. Fax: +82-2- 958- 5309.

ACKNOWLEDGMENT

The authors gratefully acknowledge the support from the KIST Institutional Program (D.Y.K.), the Korea Research Council of Fundamental Science & Technology (KRCF) (D.K.) and KIST for 'National Agenda Project (NAP)' program (S.Y.J.).

REFERENCES

(1) O'Regan, B.; Gratzel, M. *Nature* **1991**, *353*, 737–740.
(2) Hagfeldt, A.; Boschloo, G.; Lindström, H.; Figgemeier, E.; HolmbeArg, A.; ranyos, V.; Magnusson, E.; Malmqvist, L. *Cord. Chem. Rev.* **2004**, *248*, 1501–1509.
(3) Gratzel, M. *Inorg. Chem.* **2005**, *44*, 6841–6851.
(4) Martinson, A. B. F.; Hamann, T, W.; Pellin, M. J.; Hupp, J. T. *Eur. J.* **2008**, *14*, 4458–4467.
(5) Bisquert, J.; Vikhrenko, V. S. *J. Phys. Chem. B* **2004**, *108*, 2313–2322.
(6) Grätzel, M. *J. Photochem. Photobiol. A: Chem.* **2004**, *164*, 3–14.
(7) Nakade, S.; Kanzaki, T.; Wada, Y.; Yanagida, S. *Langmuir* **2005**, *21*, 10803–10807.
(8) Nazeeruddin, M. K.; Kay, A.; Rodicio, I.; Humphry-Baker, R.; Mueller, E.; Liska, P.; Vlachopoulos, N.; Graetzel, M. *J. Am. Chem. Soc.* **1993**, *115*, 6382–6390.
(9) Zukalova, M.; Zukal, A.; Kavan, L.; Nazeeruddin, M. K.; Liska, P.; Gratzel, M. *Nano Lett.* **2005**, *5*, 1789–1792.
(10) Kim, I.-D.; Rothschild, A.; Lee, B. H.; Kim, D. Y.; Jo, S. M.; Tuller, H. L. *Nano Lett.* **2006**, *6*, 2009–2013.
(11) Baxter, J. B.; Aydil, E. S. *Appl. Phys. Lett.* **2005**, *86*, 053114.
(12) Law, M.; Greene, L. E.; Johnson, J. C.; Saykally, R.; Yang, P. *Nat. Mat.* **2005**, *4*, 455–459.
(13) Mor, G. K.; Shankar, K.; Paulose, M.; Varghese, O. K.; Grimes, C. A. *Nano Lett.* **2005**, *6*, 215–218.
(14) Wang, H.; Yip, C. T.; Cheung, K. Y.; Djurisic, A. B.; Xie, M. H.; Leung, Y. H.; Chan, W. K. *Appl. Phys. Lett.* **2006**, *89*, 023508.
(15) Lee, B. H.; Song, M. Y.; Jang, S.-Y.; Jo, S. M.; Kwak, S.-Y.; Kim, D. Y. *J. Phys. Chem. C* **2009**, *113*, 21453–21457.
(16) Yuhas, B. D.; Yang, P. *J. Am. Chem. Soc.* **2009**, *131*, 3756–3761.
(17) Chou, T. P.; Zhang, Q.; Fryxell, G. E.; Cao, G. Z. *Adv. Mater.* **2007**, *19*, 2588–2592.
(18) Zhu, K.; Neale, N. R.; Miedaner, A.; Frank, A. J. *Nano Lett.* **2006**, *7*, 69–74.
(19) Chen, D.; Huang, F.; Cheng, Y.-B.; Caruso, R. A. *Adv. Mater.* **2009**, *21*, 2206–2210.
(20) Kim, Y. J.; Lee, M. H.; Kim, H. J.; Lim, G.; Choi, Y. S.; Park, N.-G.; Kim, K.; Lee, W. I. *Adv. Mater.* **2009**, *21*, 3668–3673.
(21) Huang, F.; Chen, D.; Zhang, X. L.; Caruso, R. A.; Cheng, Y.-B. *Adv. Funct. Mater.* **2010**, *20*, 1301–1305.

(22) Zhang, Q.; Chou, T. P.; Russo, B.; Jenekhe, S. A.; Cao, G. *Adv. Func. Mater.* **2008**, *18*, 1654–1660.
(23) Jawork, A. *J. Mater. Sci.* **2007**, *42*, 266–297.
(24) Mazumder, M. K.; Wankum, D. L.; Sims, R. A.; Mountain, J. R.; Chen, H.; Pettit, P.; Chaser, T. *J. Electrostatics* **1997**, *40*, 369–374.
(25) Zhang, Y.; Wu, L.; Xie, E.; Duan, H.; Han, W.; Zhao, J. *J. Power Source* **2009**, *189*, 1256–1263.
(26) Fujimoto, M.; Kato, T.; Takashima, W.; Kaneto, K; Hayase, S. *J. Electrochem. Soc.* **2006**, A826–A829.
(27) Li, X.; Zhang, Y.; Zhang, Z.; Zhou., J.; Song, J.; Lu, B.; Xie, E.; Lan, W. *J. Power Source* **2011**, *196*, 1629–1644.
(28) Jaworek, A. *Powder Technol.* **2007**, *176*, 18–35.
(29) Kim, J.-S.; Chung, W.-S.; Kim, K.; Kim, D. Y.; Paeng, K.-J.; Jo, S. M.; Jang, S.-Y. *Adv. Funct. Mater.* **2010**, *20*, 3538–3546.
(30) Wang, Q.; Moser, J.-E.; Gratzel, M. *J. Phys. Chem. B* **2005**, *109*, 14945–14953.
(31) Bisquert, J. *J. Phys. Chem. B* **2001**, *106*, 325–333.
(32) Van de Lagemaat, J.; Park, N. G.; Frank, A. J. *J. Phys. Chem. B* **2000**, *104*, 2044–2052.
(33) Schlichthorl, G.; Park, N. G.; Frank, A. J. *J. Phys. Chem. B* **1999**, *103*, 782–791.
(34) Dloczik, L.; Ileperuma, O.; Lauermann, I.; Peter, L. M.; Ponomarev, E. A.; Redmond, G.; Shaw, N. J.; Uhlendorf, I. *J. Phys. Chem. B* **1997**, *101*, 10281–10289.
(35) Peter, L. M.; Walker, A. B.; Boschloo, G.; Hagfeldt, A. *J. Phys. Chem. B* **2006**, *110*, 13694–13699.
(36) Adachi, M.; Sakamoto, M.; Jiu, J.; Ogata, Y.; Isoda, S. *J. Phys. Chem. B* **2006**, *110*, 13872–13880.
(37) Kern, R.; Sastrawan, R.; Ferber, J.; Stangl, R.; Luther, J. *Electrochimica Acta* **2002**, *47*, 4213–4225.
(38) Qu, J.; Gao, X. P.; Li, G. R.; Jiang, Q. W.; Yan, T. Y. *J. Phys. Chem. C* **2009**, *113*, 3359–3363.
(39) Zhao, D.; Peng, T.; Lu, L.; Cai, P.; Jiang, P.; Bian, Z. *J. Phys. Chem. C* **2008**, *112*, 8486–8494.
(40) Wang, Z.-S.; Zhou, G. *J. Phys. Chem. C* **2009**, *113*, 15417–15421.
(41) Wang, Z.-S.; Yamaguchi, T.; Sugihara, H.; Arakawa, H. *Langmuir* **2005**, *21*, 4272–4276.